Master's thesis
Your Field

Formation of cores by merging supermassive black holes

Joonas Suortti

July 9, 2019

Tutor: prof. Smith

Censors: prof. Smith
doc. Smythe

UNIVERSITY OF HELSINKI
Department of Something

PL 42 (Kuvitteellinen katu 1)
00014 Helsingin yliopisto

“Bachelor’s degrees make pretty good placemats if you get them laminated.”

—Jeph Jacques

HELSINGIN YLIOPISTO — HELSINGFORS UNIVERSITET — UNIVERSITY OF HELSINKI

Tiedekunta — Fakultet — Faculty	Laitos — Institution — Department
Faculty of Whatever	Department of Something

Tekijä — Författare — Author

Joonas Suortti

Työn nimi — Arbetets titel — Title

Formation of cores by merging supermassive black holes

Oppiaine — Läroämne — Subject

Your Field

Työn laji — Arbetets art — Level	Aika — Datum — Month and year	Sivumäärä — Sidoantal — Number of pages
Master's thesis	July 9, 2019	0 pages

Tiivistelmä — Referat — Abstract

Abstract goes here.

Avainsanat — Nyckelord — Keywords

Your keywords here

Säilytyspaikka — Förvaringsställe — Where deposited

Muita tietoja — övriga uppgifter — Additional information

Contents

1. Introduction

2. Theory

3. KETJU

4. KETJU Results

We analyse the results from two sets of KETJU simulations of early type galaxy mergers, where the progenitor galaxies contain supermassive black holes, with masses ranging from $8.5 \times 10^8 M_\odot$ to $8.5 \times 10^9 M_\odot$, in their centre (Mannerkoski et al., 2019; Rantala et al., 2018). Apart from the central SMBH masses, the progenitor galaxies used in the simulations are identical.

4.1 Simulation Details

The results from the simulations done by Mannerkoski et al. (2019) contain only the locations, velocities and the masses of the central black holes of the progenitor galaxies at different time steps; starting from the step where the semi-major-axis of the SMBH system is $a \lesssim 5000 R_s$, where R_s is the Schwarzschild radius, up until the end of the simulation. We will show the initial conditions in more detail in the next subsection.

The simulation results of Rantala et al. (2018) consist of the properties of not only the black holes, but also the stellar particles and dark matter particles. This data comes from a single time before the merging of the black holes step at $t = 2$Gyr of in the simulation time. Once again, we will describe the initial conditions of the specific simulations in more depth later.

To make the distinction between the different type of simulation results clearer, we will be calling the results from Mannerkoski et al. (2019) "runs", as they contain

data from multiple simulation time steps; and the single time step results by Rantala et al. (2018) "snapshots".

4.2 Black Hole Trajectories

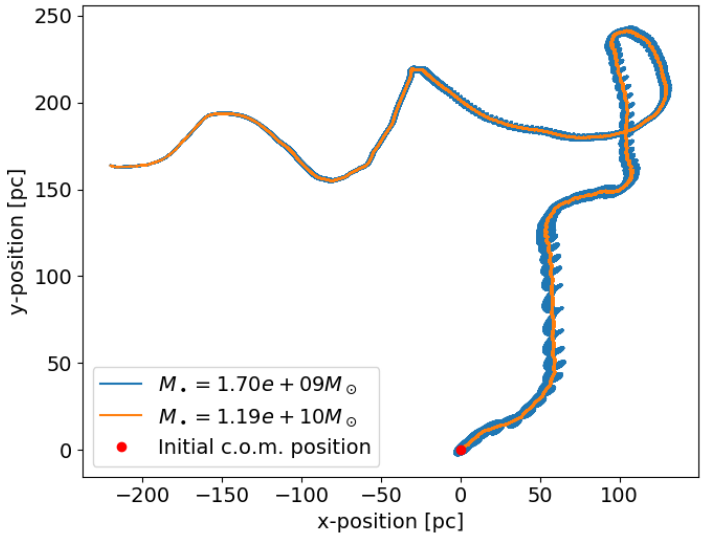

Figure 4.1: The trajectories of the black holes during "run 3" of the simulation. The coordinates are centred on the initial location of the centre-of-mass of the black hole system. The orange and blue lines show the paths taken by the smaller and larger black holes respectively during the simulation. Both paths show clear spiral patterns which become smaller and smaller as the simulation proceeds. The paths end at the location where the black holes merge, i.e. where the distance between them is below the specific threshold.

4.3 Core Radius Measurements

Since the core of a cored galaxy is defined as a deviation from the expected theoretical surface brightness profile, determining its size requires us to: not only calculate surface brightness profiles from the simulation results, but also try to model the results with theoretical models that somehow take the brightness deficiency of the

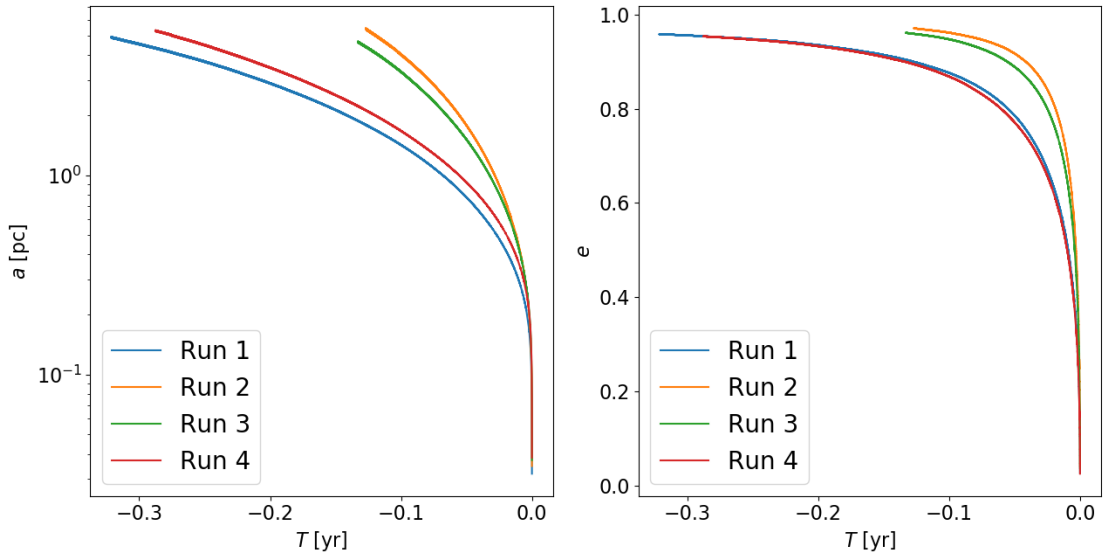

Figure 4.2: The semi-major axes (left) and eccentricities (right) of the black hole systems in simulation runs 1-4 as a function of time. The zero position on the x-axis corresponds to the point of time in the simulation, where the black hole merging event happens.

core region into account, as the starting location of the deviations from the expected can't be measured by eye.

We calculate the surface brightness profiles from the simulation snapshots by Rantala et al. (2018) by: projecting the stellar particles onto a plane and calculating the mass inside logarithmically space radial bins. In order to get a smooth density profile, we do this 100 times from random viewing angles and calculate the azimuthal averages of the binned masses. This allows us to form a mass surface density profile, which we then turn into a surface brightness profile by assuming a mass-to-light ratio of $M/L = 4$. In figure 4.3, one can see example surface brightness profiles for all of the simulated merger remnants. As can already be seen from the figure, the higher the mass of the central black holes in the progenitor galaxies, the larger the surface brightness deficiency near the center.

As stated before, in order to calculate the sizes of the cores from profiles such as the ones seen in figure 4.3, we need to fit some kind of theoretical model that can

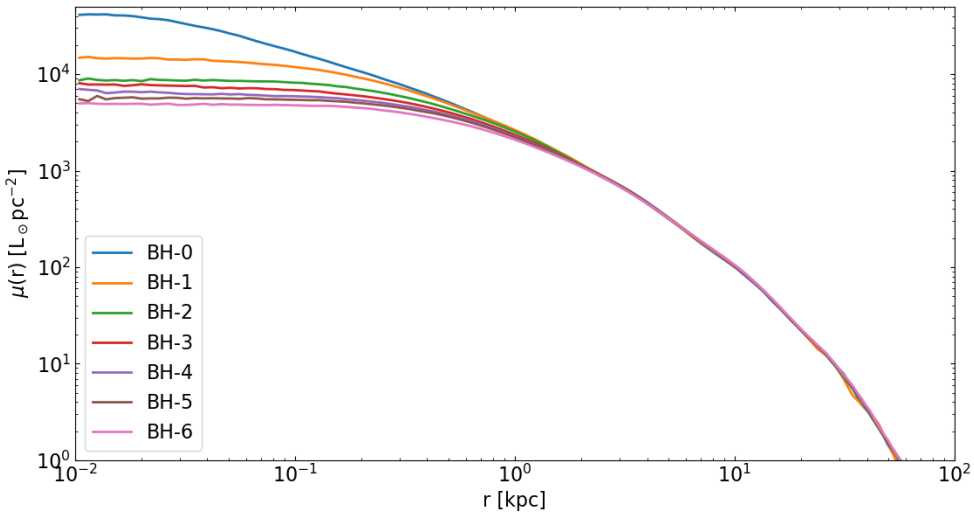

Figure 4.3: Surface brightness profiles of all of the simulated merger remnants. The profiles were calculated by dividing the remnants into 100 radial bins, and averaging the surface brightness inside the bins through 100 random viewing angles. The luminosity of the particles was estimated by assuming a mass-to-light ratio of $M/L = 4$.

describe a profile with surface brightness deficiency near the galactic centre onto the measured quantity. There are two commonly used options of profiles used for measuring the core size. The first one is the core-Sérsic profile (Graham et al., 2003):

$$\mu(r) = \mu' \left[1 + \left(\frac{r_b}{r}\right)^{\alpha}\right]^{\gamma/\alpha} \exp\left\{-b_n \left[\left(r^{\alpha} + r_b^{\alpha}\right)/r_e^{\alpha}\right]^{1/(\alpha n)}\right\}, \tag{4.1}$$

which divides the single power law Sérsic profile into a combination of an inner and outer power-law, and where r_b is the break radius (i.e. the core radius), γ is the logarithmic slope of the inner power-law, α controls the sharpness of the transition between the two power-laws, r_e and n are the effective half-mass radius and the Sérsic index of the outer power-law, and μ' is defined by:

$$\mu' = \mu_b 2^{-\gamma/\alpha} \exp\left[b_n \left(2^(1/\alpha) r_b/r_e\right)^{1/n}\right], \tag{4.2}$$

where μ_b is the surface brightness at the break radius.

The second option for calculating the core radius is the so called Nuker profile

(Lauer et al., 1995):

$$\mu(r) = 2^{(\beta-\gamma)/\alpha}\mu_b \left(\frac{r_b}{r}\right)^{\gamma} \left[1 + \left(\frac{r}{r_b}\right)^{\alpha}\right]^{(\gamma-\beta)/\alpha}, \tag{4.3}$$

where r_b is once again the break radius (core radius), μ_b is the surface brightness at the core radius, β and γ are the logarithmic slopes of the power-laws inside and outside of the break radius respectively, and α is the sharpness of the transition between the two slopes.

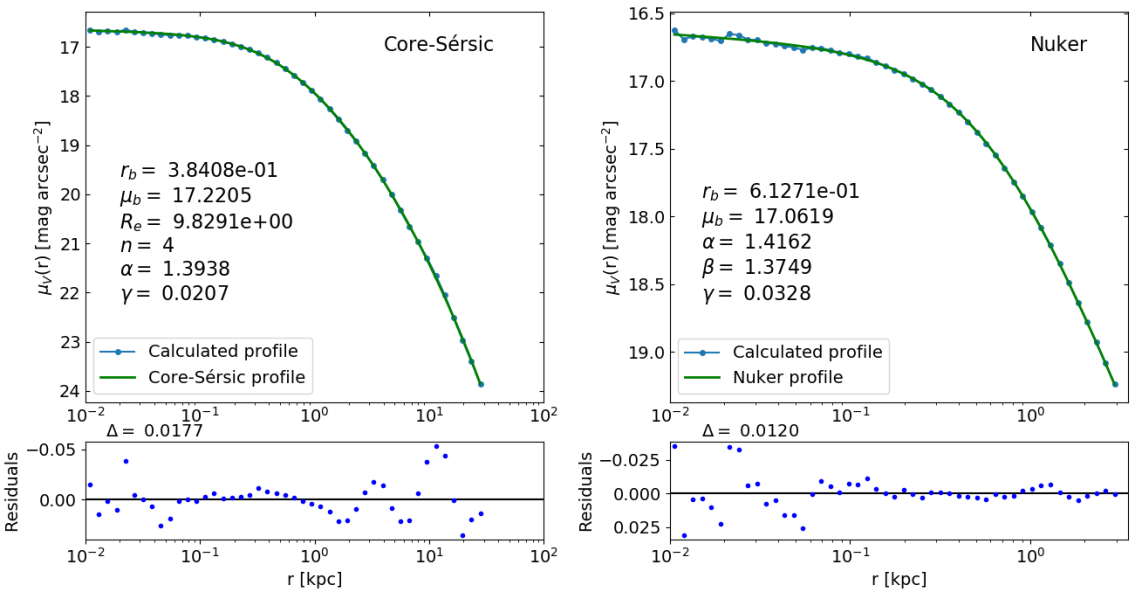

Figure 4.4: Core-Sérsic and Nuker profile fits of surface brightness profiles calculated from the result of a merger simulation with progenitors containing $3.4 \times 10^9 M_\odot$ mass central black holes (top-left and top-right figures). The best fit parameters are written on the figures, and are in the same units as the axes (i.e. r_b and R_e in kilo-parsecs, and μ_b in V-band magnitudes per arc-second squared). The residuals of the fits are plotted under their respective figures. The delta describes the root-mean-square of the residuals.

Galaxy	$M_\star$	$M_\bullet$	R_e	μ_e	n	$\langle V_{\rm LOS}\rangle$	σ_e	λ_e	ϵ_e
	$[\times 10^{11} M_\odot]$	$[\times 10^{10} M_\odot]$	[kpc]	[mag/arcsec^2]		[km/s]	[km/s]		
(1)	(2)	(3)	(4)	(5)	(6)	(7)	(8)	(9)	(10)
BH-6	4.960	2×0.85	5.507	20.26	4	6.9	311	0.024	0.11
NGC 1600	5.0	1.7	~ 16	(22.53)	5.83	3.4	293	0.026	032

Table 4.1: Comparison between the physical properties of the simulated merger remnant "BH-6" and the galaxy NGC 1600. The properties described in the columns of the table are explained below, with the sources for the properties of NGC 1600 being written inside the brackets.

(1) Name of the galaxy.

(2) Total stellar mass (Thomas et al., 2016).

(3) Central black hole mass (Thomas et al., 2016).

(4) Effective radius (Thomas et al., 2016). For NGC 1600, the effective radius is changed from arc seconds to kpc by assuming that it is located at the distance of $D = 64$ Mpc (Thomas et al., 2016).

(5) Surface brightness at the effective radius.

(6) Sérsic index from the best fitting core-Sérsic profile fit (Thomas et al., 2016).

(7) Mean line-of-sight velocity inside the effective radius (Bender et al., 1994).

(8) Velocity dispersion inside the effective radius (Veale et al., 2017). For "BH-6", the given velocity dispersion is calculated from a Voronoi binned image as the mean of the velocity dispersion values of the bins located inside the effective radius.

(9) Spin parameter at the effective radius (Veale et al., 2018).

(10) For "BH-6": ellipticity of the galaxy at the effective radius; and for GC 1600: luminosity weighted ellipticity (Goullaud et al., 2018).

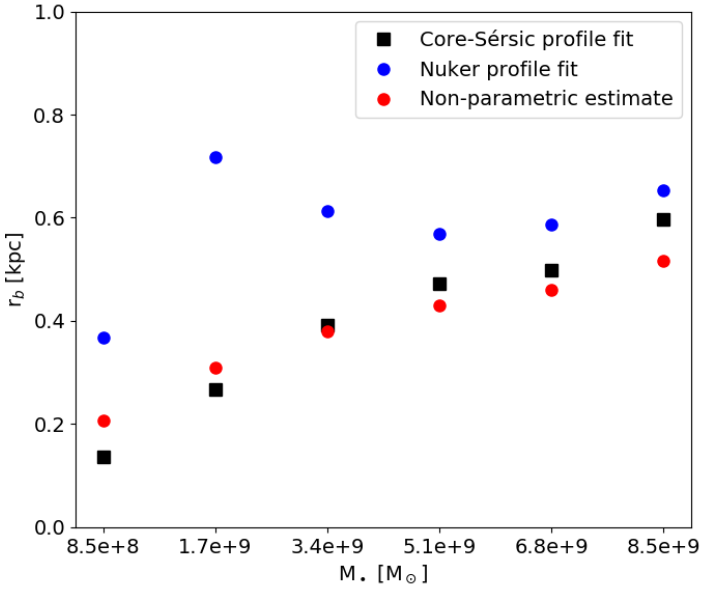

Figure 4.5: Comparison of core radii of the merger remnants, gained through three different methods; Core-Sérsic profile fitting (black squares), Nuker profile fitting (blue circles) and using equation (tähän kaava!) for finding the "cusp radius" (red circles).

4.4 Kinematic Properties

4.5 Comparison to Observations

4.6 Implications

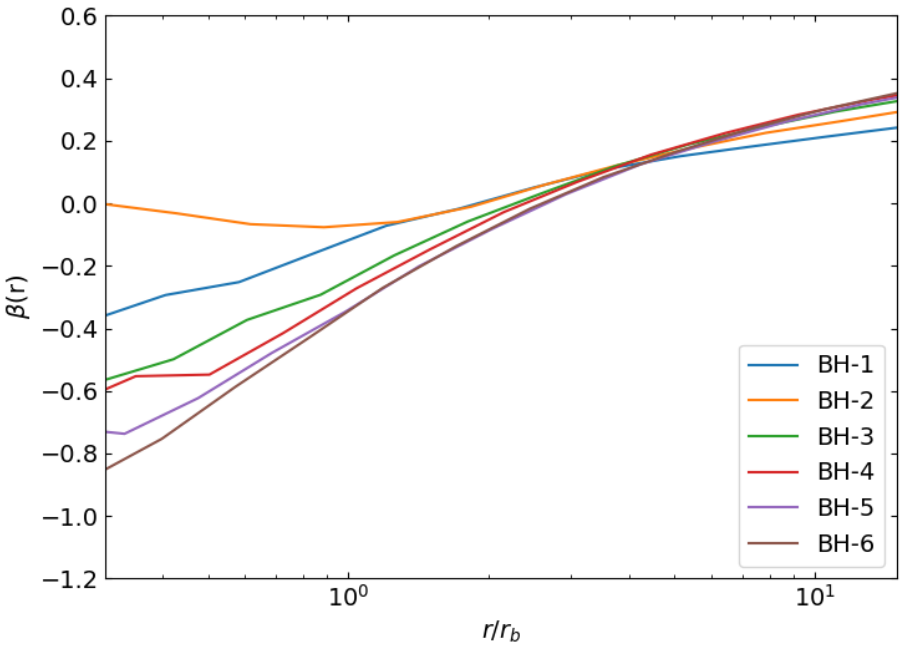

Figure 4.6: Velocity anisotropy (beta) profiles of the simulated merger remnants with central black holes.

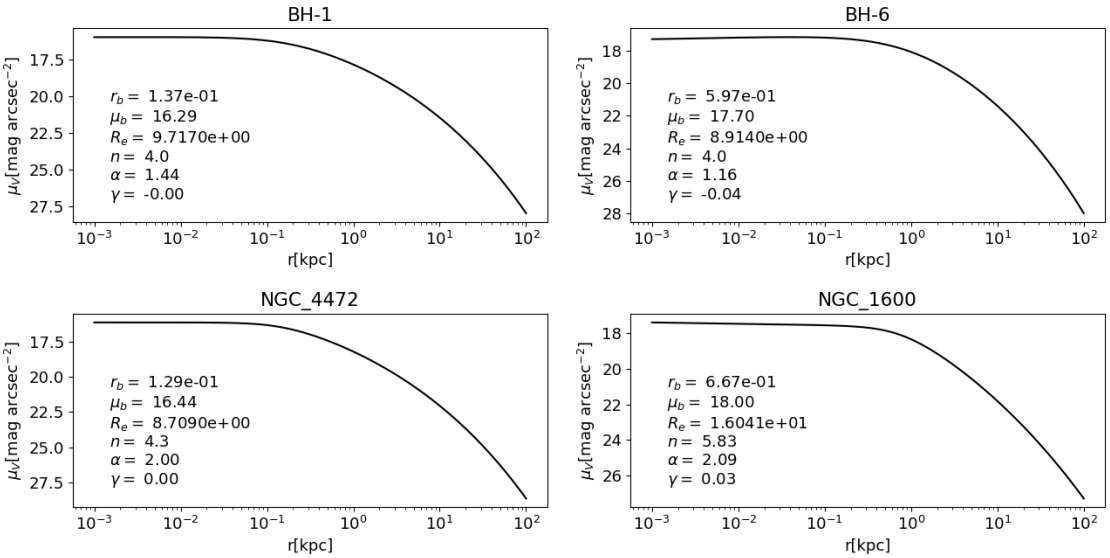

Figure 4.7: Core-Sérsic profile fits of surface brightness profiles calculated from either merger simulation results (top figures) or observed galaxies (bottom figures). The respective fit parameters are written on the figures in units that correspond to the axes. The progenitors of the top-left simulation contained $8.5 \times 10^8 M_\odot$ mass central SMBHs, and $8.5 \times 10^9 M_\odot$ mass central SMBHs in the top-right simulation. The parameters for NGC1600's profile (bottom right), are changed from the units used by Thomas et al. (2016) to the above by assuming $V - R = 0.5$ (the same assumption being done by Lauer et al. (2007)), and by using the distance $D = 64$Mpc (Thomas et al., 2016) in order to define the relation between arc seconds and parsecs. As one can see, the profiles gained from simulations and observations are quite similar to each other.

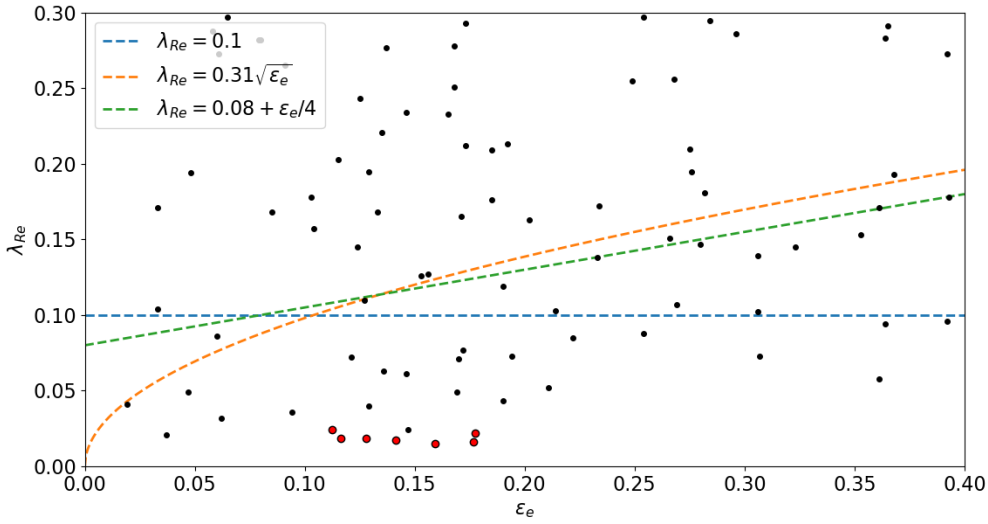

Figure 4.8: The values of the λ_{Re}-parameter of galaxies, plotted against their ellipticity at the effective radius. The red dots correspond to the simulated merger remnants, where as the black dots correspond to galaxies observed in the ATLAS^{3D}-survey (Emsellem et al., 2011). The dashed lines display different slow rotator thresholds as a function of ellipticity.

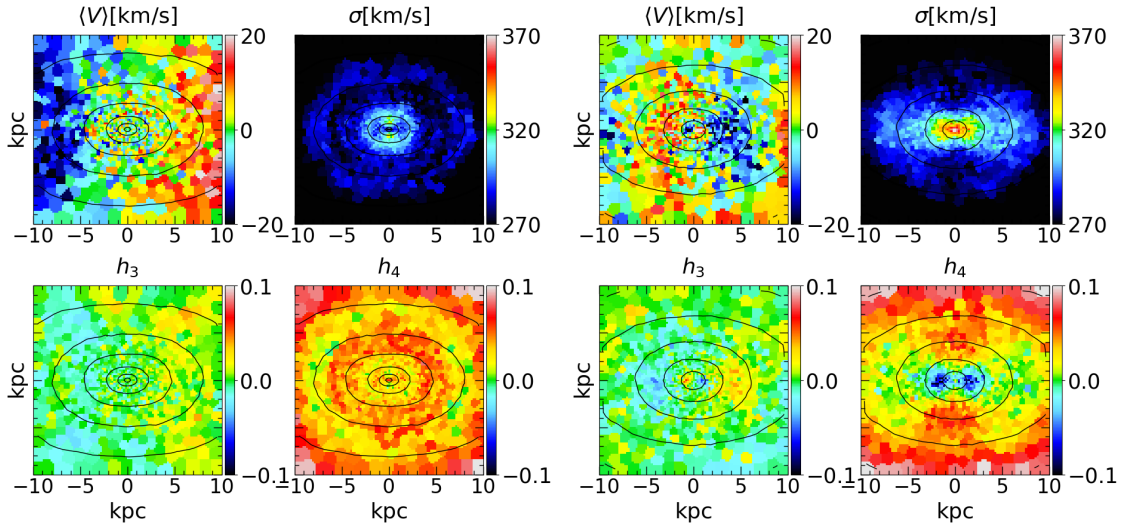

(a) BH-0 **(b)** BH-6

Figure 4.9: IFU-maps of average LOS-velocities, velocity dispersion, h_3 parameters and h_4 parameters from two simulated merger remnants. The four maps on the left are from a merger simulation where the progenitor galaxies had no central SMBHs, where as the four on the right are from a simulation with progenitor galaxies containing $M_\bullet = 8.5 \times 10^9 M_\odot$ central black holes.

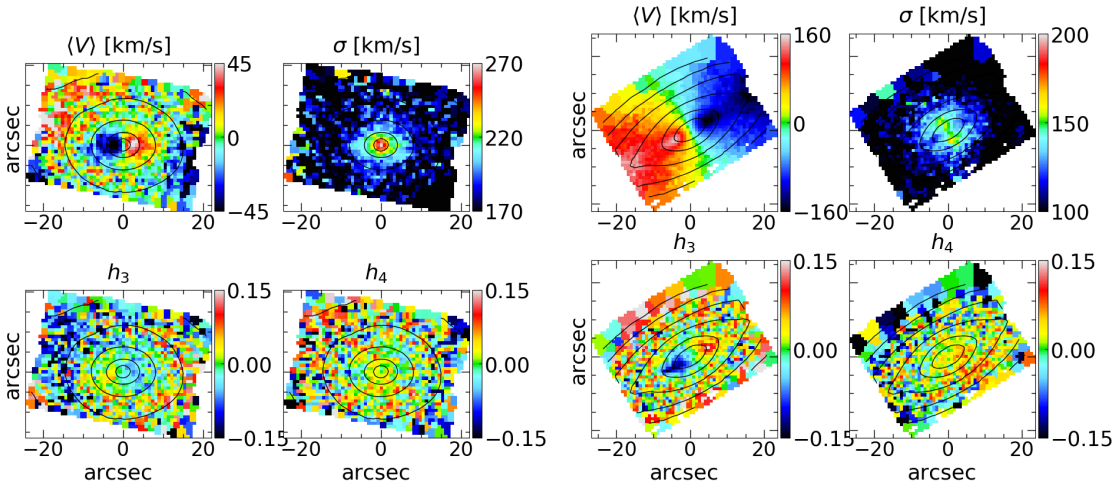

(a) NGC 3414 **(b)** NGC 4111

Figure 4.10: IFU-maps of average LOS-velocities, velocity dispersion, h_3 parameters and h_4 parameters from ATLAS3D observations of two galaxies (NGC 3414 (Emsellem et al., 2004) and NGC 4111 (Cappellari et al., 2011)).

5. Conclusions

Bibliography

R. Bender, R. P. Saglia, and O. E. Gerhard. Line-of-sight velocity distributions of elliptical galaxies. *Monthly Notices of the Royal Astronomical Society*, 269: 785–813, Aug 1994. doi: 10.1093/mnras/269.3.785.

M. Cappellari, E. Emsellem, D. Krajnović, R. M. McDermid, N. Scott, G. A. Verdoes Kleijn, L. M. Young, K. Alatalo, R. Bacon, L. Blitz, M. Bois, F. Bournaud, M. Bureau, R. L. Davies, T. A. Davis, P. T. de Zeeuw, P.-A. Duc, S. Khochfar, H. Kuntschner, P.-Y. Lablanche, R. Morganti, T. Naab, T. Oosterloo, M. Sarzi, P. Serra, and A.-M. Weijmans. The ATLAS^{3D} project - I. A volume-limited sample of 260 nearby early-type galaxies: science goals and selection criteria. *Monthly Notices of the Royal Astronomical Society*, 413:813–836, May 2011. doi: 10.1111/j.1365-2966.2010.18174.x.

E. Emsellem, M. Cappellari, R. F. Peletier, R. M. McDermid, R. Bacon, M. Bureau, Y. Copin, R. L. Davies, D. Krajnović, H. Kuntschner, B. W. Miller, and P. T. de Zeeuw. The SAURON project - III. Integral-field absorption-line kinematics of 48 elliptical and lenticular galaxies. *Monthly Notices of the Royal Astronomical Society*, 352:721–743, August 2004. doi: 10.1111/j.1365-2966.2004.07948.x.

E. Emsellem, M. Cappellari, D. Krajnović, K. Alatalo, L. Blitz, M. Bois, F. Bournaud, M. Bureau, R. L. Davies, T. A. Davis, P. T. de Zeeuw, S. Khochfar, H. Kuntschner, P.-Y. Lablanche, R. M. McDermid, R. Morganti, T. Naab,

T. Oosterloo, M. Sarzi, N. Scott, P. Serra, G. van de Ven, A.-M. Weijmans, and L. M. Young. The ATLAS^{3D} project - III. A census of the stellar angular momentum within the effective radius of early-type galaxies: unveiling the distribution of fast and slow rotators. *Monthly Notices of the Royal Astronomical Society*, 414:888–912, June 2011. doi: 10.1111/j.1365-2966.2011.18496.x.

Charles F. Goullaud, Joseph B. Jensen, John P. Blakeslee, Chung-Pei Ma, Jenny E. Greene, and Jens Thomas. The MASSIVE Survey. IX. Photometric Analysis of 35 High-mass Early-type Galaxies with HST WFC3/IR. *The Astrophysical Journal*, 856(1):11, March 2018. doi: 10.3847/1538-4357/aab1f3.

Alister W. Graham, Peter Erwin, I. Trujillo, and A. Asensio Ramos. A New Empirical Model for the Structural Analysis of Early-Type Galaxies, and A Critical Review of the Nuker Model. *The Astronomical Journal*, 125(6):2951–2963, Jun 2003. doi: 10.1086/375320.

T. R. Lauer, E. A. Ajhar, Y. I. Byun, A. Dressler, S. M. Faber, C. Grillmair, J. Kormendy, D. Richstone, and S. Tremaine. The Centers of Early-Type Galaxies with HST.I.An Observational Survey. *The Astronomical Journal*, 110:2622, Dec 1995. doi: 10.1086/117719.

Tod R. Lauer, Karl Gebhardt, S. M. Faber, Douglas Richstone, Scott Tremaine, John Kormendy, M. C. Aller, Ralf Bender, Alan Dressler, and Alexei V. Filippenko. The Centers of Early-Type Galaxies with Hubble Space Telescope. VI. Bimodal Central Surface Brightness Profiles. *The Astrophysical Journal*, 664(1):226–256, July 2007. doi: 10.1086/519229.

Matias Mannerkoski, Peter H. Johansson, Pauli Pihajoki, Antti Rantala, and Naab Thorsten. Inspiral of Supermassive Black Holes In Galactic Scale Simulations. *Monthly Notices of the Royal Astronomical Society*, 856(1):11, ? 2019. doi: 10.3847/1538-4357/aab1f3.

Antti Rantala, Peter H. Johansson, Thorsten Naab, Jens Thomas, and Matteo Frigo. The Formation of Extremely Diffuse Galaxy Cores by Merging Supermassive Black Holes. *The Astrophysical Journal*, 864(2):113, September 2018. doi: 10.3847/1538-4357/aada47.

Jens Thomas, Chung-Pei Ma, Nicholas J. McConnell, Jenny E. Greene, John P. Blakeslee, and Ryan Janish. A 17-billion-solar-mass black hole in a group galaxy with a diffuse core. *Nature*, 532(7599):340–342, April 2016. doi: 10.1038/nature17197.

Melanie Veale, Chung-Pei Ma, Jens Thomas, Jenny E. Greene, Nicholas J. McConnell, Jonelle Walsh, Jennifer Ito, John P. Blakeslee, and Ryan Janish. The MASSIVE Survey - V. Spatially resolved stellar angular momentum, velocity dispersion, and higher moments of the 41 most massive local early-type galaxies. *Monthly Notices of the Royal Astronomical Society*, 464(1):356–384, January 2017. doi: 10.1093/mnras/stw2330.

Melanie Veale, Chung-Pei Ma, Jenny E. Greene, Jens Thomas, John P. Blakeslee, Jonelle L. Walsh, and Jennifer Ito. The MASSIVE survey - VIII. Stellar velocity dispersion profiles and environmental dependence of early-type galaxies. *Monthly Notices of the Royal Astronomical Society*, 473(4):5446–5467, February 2018. doi: 10.1093/mnras/stx2717.